Drug Delivery Hot Paper

Tuning the Elasticity of Nanogels Improves Their Circulation Time by Evading Immune Cells

Prachi Desai, Rahul Rimal, Alexandru Florea, Rustam A. Gumerov, Marta Santi, Anastasia S. Sorokina, Sabri E. M. Sahnoun, Thorsten Fischer, Felix M. Mottaghy, Agnieszka Morgenroth, Ahmed Mourran, Igor I. Potemkin, Martin Möller, and Smriti Singh*

Abstract: Peptide receptor radionuclide therapy is used to treat solid tumors by locally delivering radiation. However, due to nephro- and hepato-toxicity, it is limited by its dosage. To amplify radiation damage to tumor cells, radiolabeled nanogels can be used. We show that by tuning the mechanical properties of nanogels significant enhancement in circulation half-life of the gel could be achieved. We demonstrate why and how small changes in the mechanical properties of the nanogels influence its cellular fate. Nanogels with a storage modulus of 37 kPa were minimally phagocytosed by monocytes and macrophages compared to nanogels with 93 kPa modulus. Using PET/CT a significant difference in the blood circulation time of the nanogels was shown. Computer simulations affirmed the results and predicted the mechanism of cellular uptake of the nanogels. Altogether, this work emphasizes the important role of elasticity even for particles that are inherently soft such as nano- or microgels.

Introduction

Currently, peptide receptor radionuclide therapy (PRRT) is used to treat solid tumors by delivering radiation that targets specific receptors highly expressed in the tumor cells compared to healthy cells. Although PRRT holds promising advancement in nuclear medicine, it suffers from limitations such as nephron and hepato-toxicity, which restricts its applied dose. To improve the efficacy of PRRT, nano-carriers have gained attention due to their ability to decrease non-specific organ accumulation and improve the biodistribution and therapeutic effects of the radionuclide.[1] Mononuclear phagocyte system (MPS) which mainly comprises of monocytes, macrophages, and bone marrow progenitors, among which monocytes and macrophages remain a major barrier for the delivery of nanocarriers. To evade the uptake by MPS, physicochemical properties of the nanocarriers are tuned to achieve the optimum therapeutic efficacy. Size, shape, surface charge, and hydrophilicity/hydrophobicity are very well-investigated properties that influence tumor accumulation, circulation time, MPS evasion, renal clearance, and cellular uptake.[2] However, the influence of nanocarrier mechanical properties on its biopharmaceuticals has recently gained attention. The effects of physical properties (material elasticity) on biological responses come from biology itself. Mechanical signals transmitted by change in cytoskeletal network of the cells are transduced to a biochemical response, for instance, erythrocytes stiffens upon aging and are soft during circulation, thus squeezing through capillaries as narrow as 1.8 μm.[3] Once stiff, they lose their deformable property and are eventually cleared via the spleen.[4] In addition, the influence of substrate stiffness on particle uptake is also investigated highlighting the importance of elasticity.[5] These studies emphasize the role of mechanical properties in regulating biological processes.

[*] P. Desai, R. Rimal, Dr. R. A. Gumerov, M. Santi, T. Fischer,
Dr. A. Mourran, Prof. I. I. Potemkin, Prof. M. Möller, Dr. S. Singh
DWI Leibniz Institute for Interactive Materials e.V,
RWTH Aachen University
Forckenbeckstrasse 50, 52074 Aachen (Germany)

Dr. S. Singh
Max Planck Institute for Medical Research (MPImF)
Jahnstrasse 29, 69120 Heidelberg (Germany)
E-mail: smriti.singh@mr.mpg.de

Dr. A. Florea, S. E. M. Sahnoun, Prof. F. M. Mottaghy,
Dr. A. Morgenroth
Department of Nuclear Medicine,
University Hospital RWTH Aachen
Pauwelstraße 30, 52074 Aachen (Germany)

Dr. A. Florea, Prof. F. M. Mottaghy
Department of Radiology and Nuclear Medicine,
School for Cardiovascular Diseases (CARIM) and School for
Oncology (GROW), Maastricht University
6229 HX Maastricht (The Netherlands)

Dr. R. A. Gumerov, A. S. Sorokina, Prof. I. I. Potemkin
Physics Department, Lomonosov Moscow State University
Leninskie Gory 1–2, 119991 Moscow (Russian Federation)

Prof. I. I. Potemkin
National Research South Ural State University
Chelyabinsk 454080 (Russian Federation)

Recently, nanocarriers such as hydrogel nanoparticles[4,6] and microparticles,[7] nanoliposomes,[8] Polymeric nanoparticles,[9] and silica nanocapsules[10] with elasticities ranging from 1.3 kPa to 9 GPa have been developed and the effect of varying the mechanical properties on cellular uptake was investigated.[11] However, these studies mainly focus on comparing a broad elasticity range, which tends to show a significant difference in vitro and in vivo. However, a study by Banquy et al. showed an increase in hydrogel nanoparticles uptake by macrophages of varying elasticities in the range 18–210 kPa. Although this study focusses on a narrow elasticity range, it lacks to elucidate how small changes in mechanical properties of a nanocarrier can influence its in vivo fate.[6a]

In this work we demonstrate the synthesis of nanogels (NGs) in the elasticity range 30 kPa–95 kPa to investigate the role of NG elasticity in improving blood circulation time and hence potential radionuclide therapy. Star-shaped thiol functionalized poly(ethylene glycol) pre-polymer with 6-arms (sPEG-SH) was used to develop disulfide cross-linked NG. The elasticity of the NGs was tuned by varying the number of functional thiol-groups in the pre-polymer without any alteration in polymer concentration. To maintain similar physicochemical properties, it was important to maintain similar polymer concentration as we have previously shown that changing polymer concentration affects the NG properties.[12] The mechanical properties of the NGs were quantified indirectly by measuring the bulk hydrogel at the macroscopic scale using a rheometer. Atomic force microscopy (AFM) was used to quantify the modulus of the NGs in the swollen state. Thiol-disulfide exchange is reversible in the presence of a reducing agent or cysteine molecules, which can lead to the reduction of disulfides back to thiols. Low amounts of cysteine molecules in the blood may interfere with interpreting these NG interactions in vitro and in vivo. Therefore, a soft non-reducible NG cross-linked using PEG diacrylate via Michael addition was prepared. The thioester bonds formed via Michael addition between thiols and acrylates are not reducible and thus behave as a control to associate the interaction solely based on elasticity. Furthermore, these NGs were characterized for their size, zeta potential, morphology, modulus, deformability, and radiochemical yield. To further ascertain the effect of NG elasticity on MPS uptake, flow cytometry (FACS) of the fluorescently labeled gels incubated with monocytes (THP-1), and macrophage (PMA stimulated THP-1) cells were performed. Computer aided simulations were used to understand the role of NG elasticity on cellular uptake. The in vivo efficiency of radiolabeled NGs with different elasticities was evaluated in Balb/c nude mice and was visualized using a small animal PET/CT.

Results and Discussion

Interactions between a nanocarrier and an immune cell are greatly influenced by the physicochemical properties and in particular by the elasticity of the nanocarrier. Lately, the ability of macrophages to selectively phagocytose erythro-cytes with different elasticities was studied, which suggested that nanocarrier elasticity can play a role in regulating its biological events.[13] It was speculated that the forces generated by macrophages (during phagocytosis) are strong enough to deform the softer nanocarriers which in turn influences phagocytosis.[6b] In this work, we decipher why and how small changes in mechanical properties of the NGs influences its cellular fate by 1) showing the effect of NG elasticity on its deformation during phagocytosis 2) validating and demonstrating the influence of NG deformation in reducing cellular uptake in vitro and overall biodistribution in vivo.

The most commonly used approach to synthesize NGs with different elasticity is to vary the cross-linker concentration or polymer concentration. Altering the elasticity via this approach can lead to additional changes in the NG properties, resulting in inaccurate comparisons.[14] In this work, we explore the use of sPEG-SH with different arm lengths to achieve NGs with different storage modulus but with the same polymer volume fraction. For this, 3 kDa and 12 kDa, sPEG-SH were used. NGs were synthesized in an inverse miniemulsion (Figure 1A) via oxidation of thiols to disulfides using hydrogen peroxide (H_2O_2).[15] Prior to the NG synthesis, a series of disulfide cross-linked hydrogels with different polymer volume fractions of 3 kDa and 12 kDa sPEG-SH were synthesized and the storage modulus of the formed hydrogels was compared (Figure 1B). As expected, hydrogels with 3 kDa resulted in higher storage modulus compared to 12 kDa sPEG-SH hydrogels with the same volume fraction. This difference in storage modulus is attributed to the difference in thiol content, which in turn determines the crosslink density (Figure 1C). Among the range of pre-polymer concentration tested, a polymer volume fraction of 44 wt % produced two distinct storage moduli gels, the soft (37 kPa) and hard (93 kPa) with 12 and 3 kDa sPEG-SH, respectively (Figure 1B), which was further selected to synthesize NGs with different elasticities. The polymer volume fraction for the synthesis of NGs was chosen also based on the minimum functionality of the pre-polymer required to achieve sufficient radiolabeling efficiency. With the pre-polymer concentration chosen, we could tailor the modulus and still achieve ≥ 95 % radiolabeling efficiency.

The resulted NGs are referred to as hard reducible NG (93 kPa) and soft reducible NG (37 kPa). Raman spectroscopy was used to confirm NG formation, a qualitative tool that identifies the S–S stretching frequency as a sharp band near 500 cm^{-1}. From the Raman spectra, it can be observed that the SH band at 2560 cm^{-1} from sPEG-SH pre-polymer disappeared upon NG formation and distinct bands at the S–S vibration appeared (Figure 1D). Since disulfide bridge can be degraded in presence of tripeptide glutathione, for control a non-reducible soft NG (soft non-reducible NG) was synthesized by crosslinking the thiols in the pre-polymer via PEG diacrylate which resulted in thioester cross-linked NGs. The corresponding hydrogel showed comparable storage modulus as the soft reducible NGs (Figure S1A). The successful synthesis of these NGs was confirmed by Raman spectroscopy, which showed disappearance of –SH
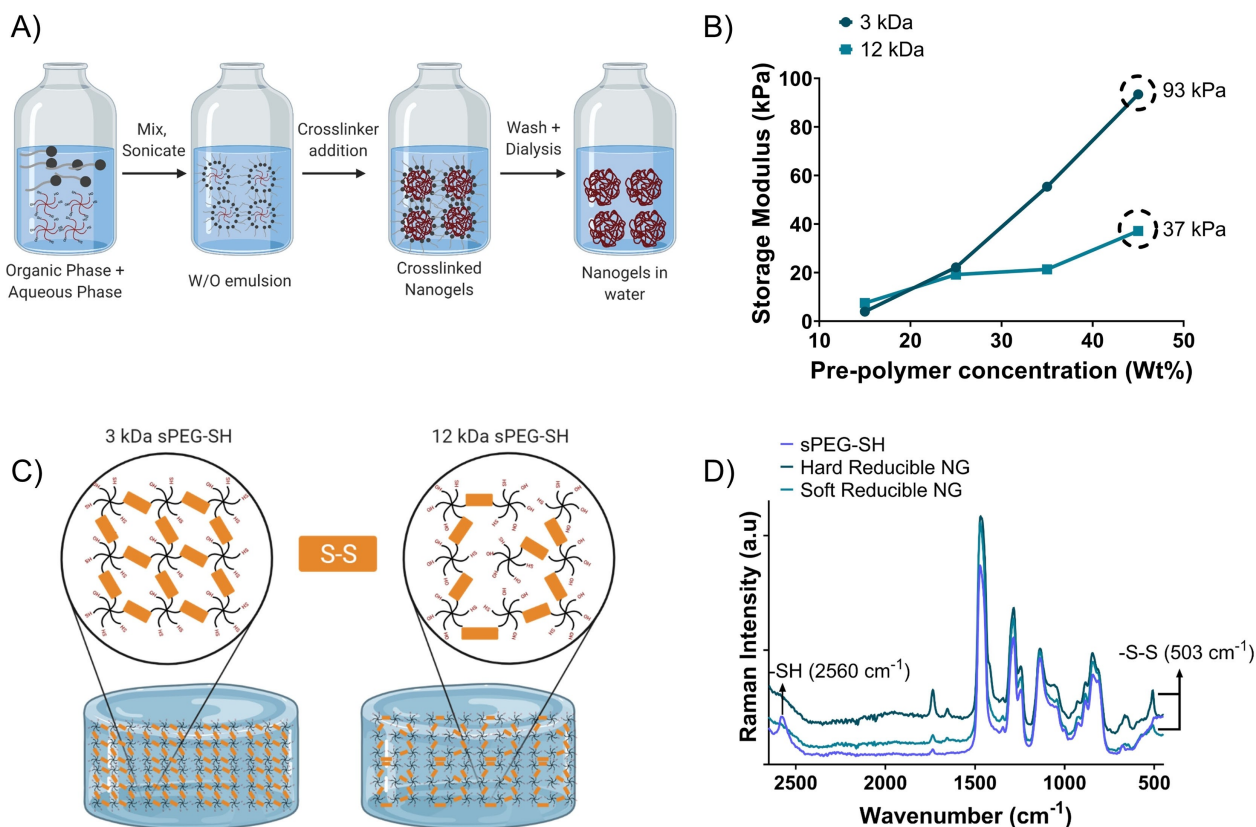
Figure 1. Synthesis of NGs with different elasticities. A) Schematic representation of nanogels synthesis via inverse miniemulsion. B) Tuning bulk hydrogel modulus over a range of pre-polymer concentrations by varying the number of functional thiol-groups. C) Schematic representation of the difference in crosslink density using two different pre-polymer molecular weights but with the same polymer volume fraction. D) Raman spectra of the nanogels which confirms NG synthesis. The thiol band at 2560 cm^{-1} disappears upon NG formation and a disulfide band at 503 cm^{-1} appears after NG synthesis.

band and presence of thioester (C–S) bond stretching vibration at 672 cm^{-1} after NG formation (Figure S1B).

NGs with different elasticities were further characterized for their physicochemical properties using diverse techniques to confirm their size, morphology, surface charge, modulus, and deformability. Dynamic light scattering (DLS) and cryo-scanning electron microscopy (Cryo-SEM) were used to characterize NG size and morphology in the swollen state. Zetasizer Nano ZS was used to measure the zeta potential of the NGs. Particle size analysis and zeta potential measurements demonstrate that all three NGs have comparable hydrodynamic diameters in the range of 280–350 nm with a PDI of < 0.3 and zeta potential in the range −13 mV to −27 mV (Figure 2A). Cryo-SEM clearly shows well-defined spherical morphology of the three NGs (Figure 2B–D) with particle diameters in the range 200 nm to 350 nm (Figure 2E–G). The NGs in general have an open structure with solvated fussy boundary in the swollen state. Thus, from the particle characterization, it is evident that this approach of varying mechanical stiffness does not change the physicochemical properties of the different NGs.

AFM measurements were performed to measure the height profile of the NGs in dry state, which determines the NG deformability and hence indicates its rigidity. From the AFM images (Figure 3A, B), we observe the difference in

the height of the hard reducible NG and soft reducible NG as demonstrated by the height profile of a single NG (Figure 3D). For better comparison, an average length-to-height ratio of 20 NG particles was calculated and plotted as the NGs ability to deform (Figure 3F). Our results indicate higher deformability of soft NG, which is due to the difference in the NG elasticities. The measure of deformability is determined by the ability of the particles to adopt a flattened, oblate spherical shape when placed on the hydrophilic mica surface. The soft reducible NGs have demonstrated an increase in diameter with a higher degree of flattening than hard NG, which indicates the higher deformability of soft NGs and its ability to flatten on a stiff substrate (Figure 3C and E).

In addition to the bulk rheological characterization, the elastic properties of a single NG in the swollen state was determined by indenting an AFM tip with a controlled force into the NG sample and measuring its deformation. This way the elastic modulus was estimated. To this end, the NGs were anchored by a dative bond on to the gold surface via the thiol moieties of the PEG chains. This allowed simultaneous imaging of the sample surface and high-resolution maps of the NG mechanical properties. Figures 4A and B clearly show that the soft reducible NG (Figure 4B) spreads and develops a flat profile near the surface when compared
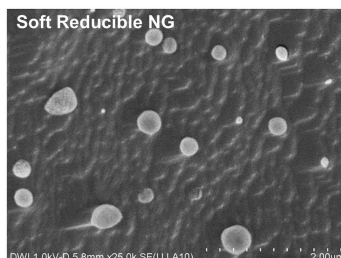
A)

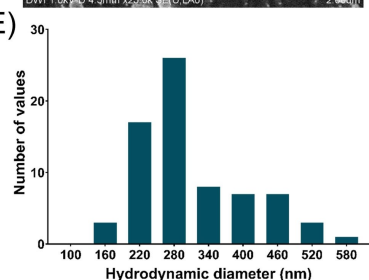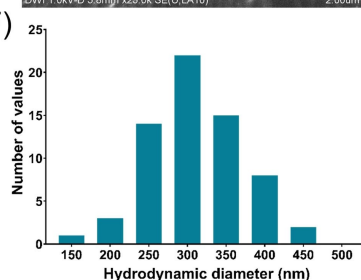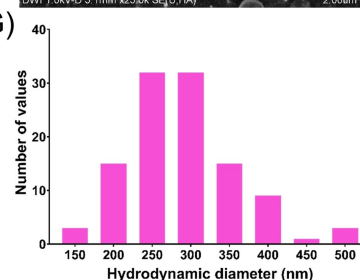| Physicochemical properties	Hard Reducible NG	Soft Reducible NG	Soft Non-Reducible NG
Hydrodynamic radius, R_h (nm)	140 ± 20	155 ± 1.6	160 ± 20
PDI	0.15	0.26	0.25
Zeta Potential (mV)	-27.3	-24.1	-13.32
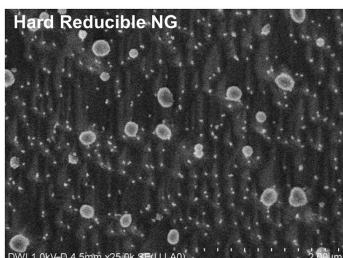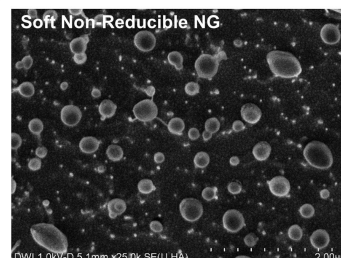
Figure 2. Characterization of three different nanogels. A) Hydrodynamic radius and Zeta potential of different nanogels showing similar physicochemical properties, with R_h in the range 140–160 nm and Zeta potential ranging from −13 to −27 mV. B), C), D) Spherical morphology of the different nanogels as demonstrated by Cryo-SEM. Scale bar: 2 μm. E), F), G) Histogram of different nanogels size analyzed from cryo-FESEM using ImageJ.

to the hard reducible NG (Figure 4A). For the soft reducible NG, a bigger particle diameter was used for determining the modulus. The reason to choose a bigger particle was mainly to eliminate the contribution from the substrate stiffness during the measurements. This first observation was made quantitatively by analyzing ≈3000 force-distance curves collected from both samples (Figure 4C and E). It is worth mentioning that during the measurement, the load was limited to 300 pN, the indentation of the AFM tip was below 20% of the NG thickness to minimize the contribution of the underlying substrate as shown in Figure 4D. The moduli for soft reducible NG was determined to be within the range 20–40 kPa, (Figure 4C), while for hard reducible NG the measured moduli was within a range of 60–140 kPa (Figure 4E). Error bars were larger for hard reducible NG, this is a consequence of higher moduli resulting in a narrower range of indentation data (within the 0–50 pN force range) from which moduli were extracted. In addition, the extent of NG deformation was determined by plotting an average length-to-height profile of the NGs (Figure S2), which again points out the higher flattening and deformation ability of the soft reducible NG.

The effect of elastic NGs was investigated in vitro using two different cell lines, (i) monocytes (THP-1) and (ii) differentiated THP-1 (macrophages). The THP-1 cells were differentiated using phorbol-12-myristate-13-acetate (PMA) to macrophage-like cells according to the procedure in the reference.[16] THP-1 cells are suspension cell line and treating the THP-1 with PMA induces cell adherence.[17] Another feature of THP-1 differentiation is the increased granularity, as demonstrated by the high side scatter (SSC) using FACS (Figure S3). Both THP-1 and stimulated THP-1 cells are involved in the clearance of foreign substances introduced into the body and are an essential factor limiting nanocarriers performance in vivo. The NGs used to study cellular internalization were labeled with Alexa fluor 488 and quantified using FACS. The cells were incubated in RPMI media with 0.5 mg mL^{-1} of Alexa fluor 488 labeled NG for 4 h and 24 h. Untreated cells were used as a negative control. Cell uptake was compared between hard reducible NG and soft reducible NG, whereas soft non-reducible NG was used as a control to eliminate the effect of disulfide reduction in vitro. The top panel shows the histogram of the NG cell uptake by THP-1 at 4 h (Figure 5A) and 24 h (Figure 5B). The Median Fluorescence Intensity (MFI) of the histogram is plotted as a bar graph, which provides quantitative information on NG internalization (Figure 5C).

The hard reducible NG showed a higher uptake by the THP-1 cells at both time points than soft reducible NG. The same trend was followed for cell uptake by stimulated THP-
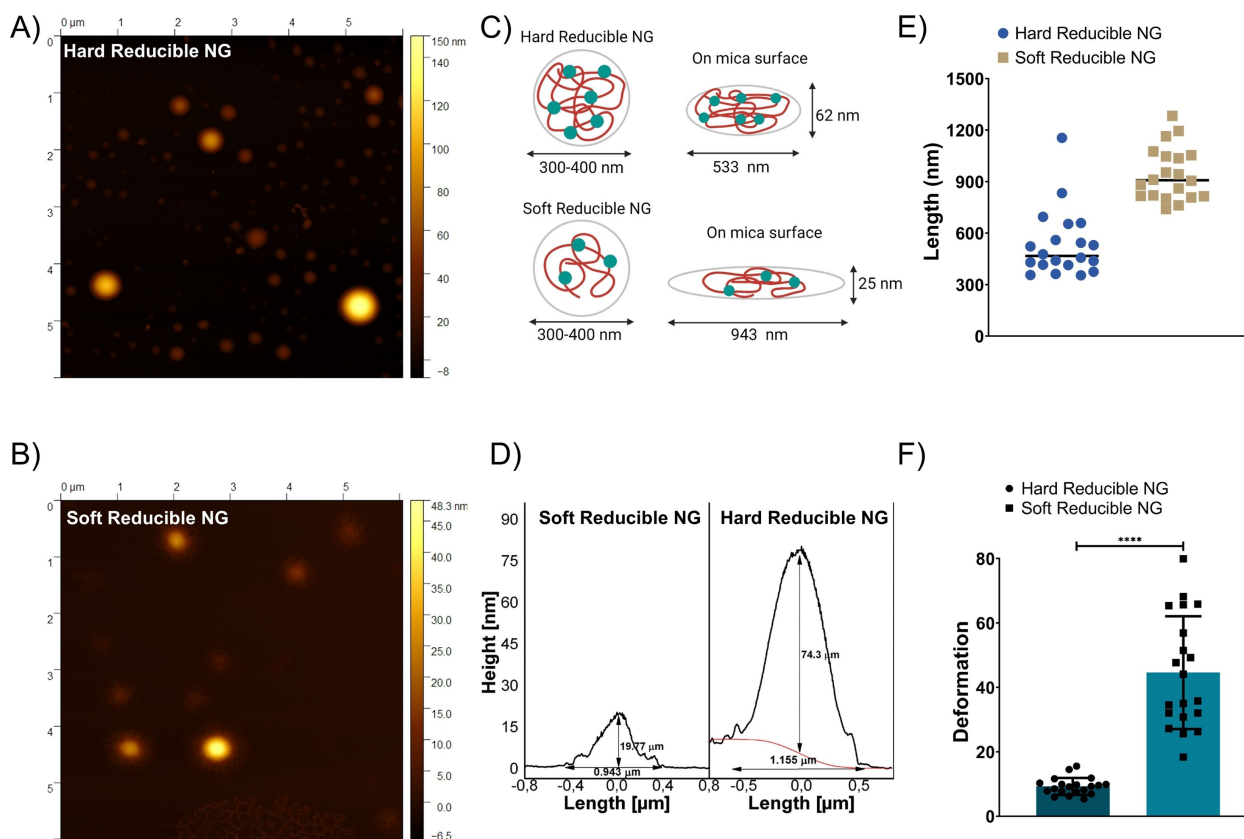
Figure 3. Height profiles of the nanogels in dry state to determine their deformability. A), B) AFM of hard and soft reducible nanogels. C) Schematic representing the behavior of elastic NGs on the mica surface. D) Height profile of a single nanogel particle. E) Lateral size of 20 random nanogels particles. F) Average deformation of nanogels from 20 particles each. **** ($p < 0.0001$) denotes statistical significance using student's t-test (two-tailed, Welch's correction).

1 (Figure 5D–F). On the other hand, no difference in uptake was observed between soft reducible NG and soft non-reducible NG, except at longer time points with THP-1 cells, which could be due to the difference in uptake mechanism. Our data lies in agreement with previous findings, showing that hard nanocarriers are phagocytosed more compared to soft nanocarriers.[18] Non-targeted uptake of the nanoparticles is generally mediated by macropinocytosis, which is an actin dependent process (Figure 6C, D). To confirm the cellular uptake mechanism we blocked the actin polymerization by pretreating the stimulated THP-1 cells with Cytochalasin D (CytD), an actin polymerization inhibitor. This pre-treatment reduced the respective initial (without pre-treatment) NG uptake by 80% (Figure 6A, B), which corroborates macropinocytosis as the main mechanism for NG uptake.

Taking into account these findings, we hypothesize that NG deformation due to differences in elasticities is augmented by actin polymerization in the cell membrane. For a cell membrane to engulf a particle passively three important energy contributions play a role:[19] a) the adhesive interaction between a particle and cell membrane, b) the bending modulus of the membrane which determines membrane's resistance to deformation, and c) membrane surface tension (see Supporting Information, computer simulations).[19] The

presence of actin filaments enhances the bending modulus of the membrane by adding force in the order of 9 pN[20] and also provides a stiffer substrate for further deformation of the NGs.[21] For a complete wrapping of the particle, the adhesive energy between the particle and the membrane must be high enough to surpass the energy cost associated with the membrane to bend around the particle.[19,22] Since actin polymerization leads to an increase in bending modulus of the membrane, the requirement of high adhesive interaction to enforce wrapping of the NGs further increases. However, because of the highly hydrophilic nature of PEG based NGs it will tend to have low adhesive interaction with the membrane. Additionally, higher deformation of soft NGs compared to its stiffer counterpart increases its contact area with the cell membrane. This large deformation of soft NGs (representing an ellipsoidal shape) requires more energy than hard NGs (representing spherical shape) for membrane wrapping, which further adds up towards the adhesion energy to complete the engulfment process.[23] Therefore, this discord between high energy barrier requirement due to NGs deformation and low adhesion energy between PEG and the cell membrane impedes the full wrapping of soft NGs, demonstrating the role of NG deformation in cellular uptake. Thus, compared
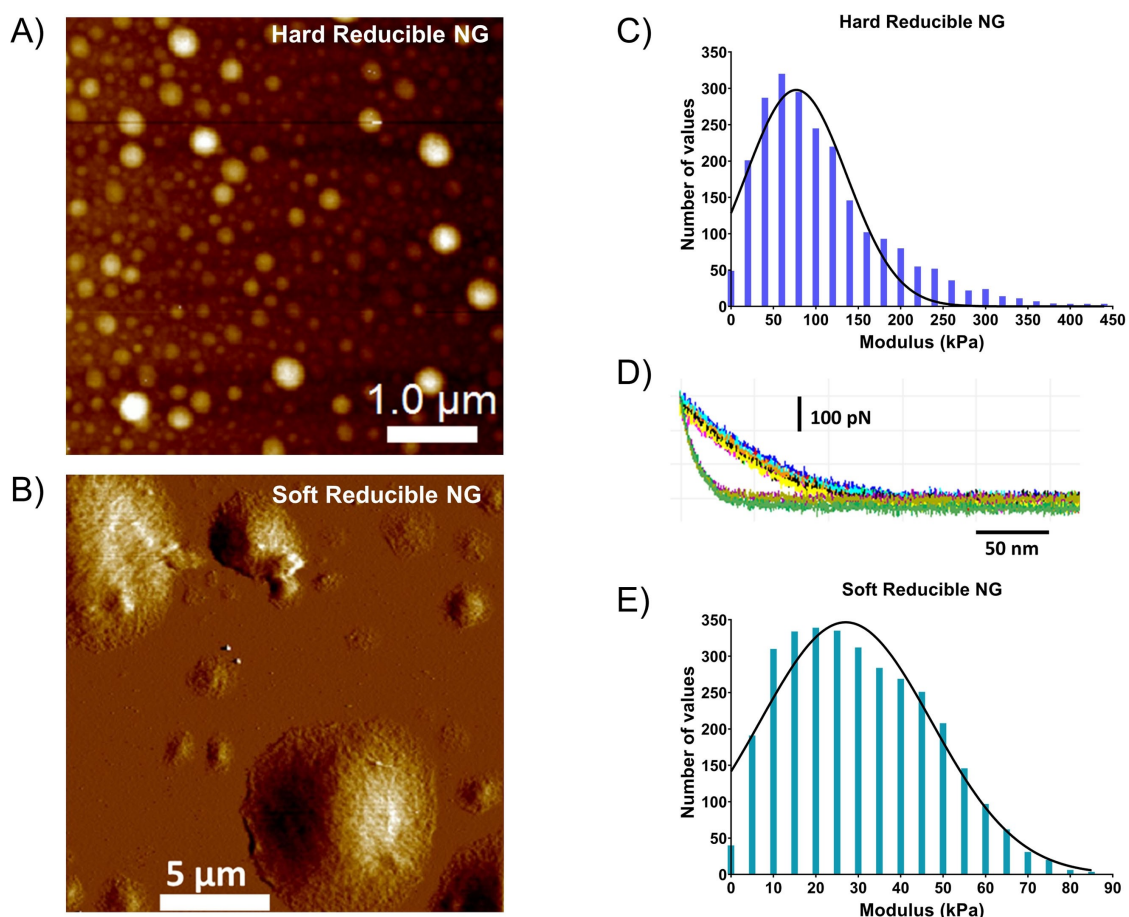
Figure 4. AFM peak force measurement in the swollen state. A), B) Topography image obtained with peak force microscopy at the water-gold interface and C), E) Young's modulus histograms (mapped to the topography images) of hard reducible NG (C) and soft reducible NG (E). The Young's modulus was calculated by analyzing 3000 force–distance (F)–(D) curves collected during the AFM imaging. D) Rrepresentative force–distance curves taken at the apex of the soft reducible NG relative to the solid support.

to soft NGs, their harder counterpart present a better chance for internalization[22,24]

Furthermore, we evaluated the uptake of hard and soft reducible NG by TEM, which again confirmed the lower uptake of soft reducible NG (Figure S4A, B). Figure S4A (i) and B (i) show the magnified images. The number of particles internalized was counted from 10 images using ImageJ and plotted as 'Number of Internalized NGs' (Figure S4C). In addition, the length (nm) of the NG was measured using ImageJ along 3 directions (vertical, horizontal, and diagonal) as an additional parameter to provide proof of internalized NGs. Out of all the values obtained, 15 values were randomly chosen and plotted (Figure S4D).

To confirm our hypothesis about the behavior of soft and hard NGs, the mesoscopic computer simulations of the adsorption of single particles onto the lipid membrane were performed.[25] We simulated the PEG NGs, which have the same hydrodynamic radii in the swollen state (≈ 15 nm) and differ in the cross-linking density (5% for the soft network and 10% for the hard network). In turn, the membrane is modeled as a bilayer composed of lipids of a single sort. The results depicting the side views of NGs at different simulation times, the number of contacts between NG

segments and lipid heads, and wrapping ratio as functions of simulation time are shown in Figure 7. Additional snapshots with top and bottom views can be found in Figures S7 and S8. Here the adsorption is the result of effective attraction between the NG segments and lipid heads (see the Supporting Information for the details). As it can be seen, the interaction with the membrane results in the deformation of both hard and soft particles, and in the latter case, a flattened "fried egg" conformation is already obtained at $t = 15$ µs (Figure 7B and Figure S8). However, for hard NGs the further interaction with the lipid heads results in the continuous engulfing of the particle (Figures 7A, S7) while for soft NGs the conformation changes weakly within the considered simulation time. Meanwhile, the number of NG-lipid head contacts is bigger for soft particles until $t \approx 200$ µs and grows slowly than for hard particles, while the wrapping ratio does not exceed 70% (Figure 7C, D). Oppositely, for hard NGs the wrapping ratio continuously increases in time as well as the number of contacts, which eventually leads to endocytosis. In other words, the softer the NGs, the longer the membrane uptake time, which correlates with the results obtained for lipid-coated core–shell nanoparticles[23] and nanoparticles of different elasticity.[26] In addition, the
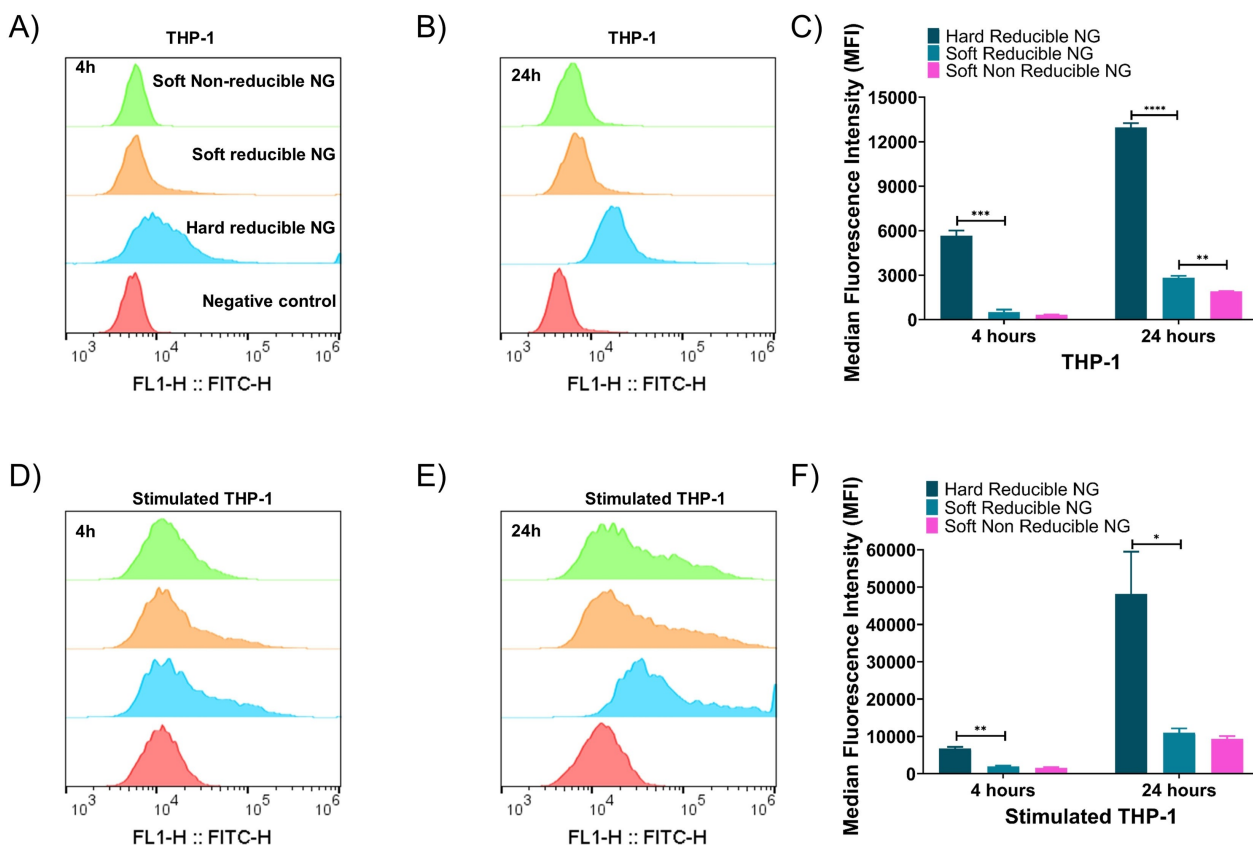
Figure 5. Cellular uptake of Alexa Fluor 488 labeled nanogels. A), B), D), and E) flow cytometry histogram of cellular uptake of different nanogels at 4 h and 24 h, respectively, by THP-1 cells and stimulated THP-1 cells showing higher uptake by the hard nanogels (as demonstrated by an increase in forward scatter). C), F) MFI of the nanogels uptake by THP-1 and stimulated THP-1, respectively ($n=3$). **** ($p < 0.0001$), *** ($p < 0.001$), ** ($p < 0.01$), * ($p < 0.05$) denotes statistical significance using student's t-test (two-tailed, Welch's correction) between hard reducible and soft reducible NG, soft reducible and soft non-reducible NG.

wrapping time for hard NG correlates well with the time obtained for elastic particles of bigger size in terms of Brownian motion scaling.[26] Interestingly, for hard NGs the engulfing process results in the non-spherical coating of the vesicle (Figure S9) which is not observed in the case of solid nanoparticles. This effect is due to the attraction between the lipid heads and the network segments and the deformability of the network. Moreover, the complete wrapping does not expel the water from NG's interior, which also can be seen in Figure S9. This validates that the NG elasticity plays a role in its deformation during phagocytosis and this deformation in turn slows or reduces the cellular uptake. Though the size of simulated NGs is significantly smaller than in the experiments, one may expect that their relative shape deformations will be similar regardless of NG's size which has been previously shown for the case of liquid–liquid[27] and liquid–solid[28] interfaces. Thus, the behavior of simulated NGs can explain the drastic difference in the cellular uptake for soft and hard samples (Figure 5).

The circulation time of hard and soft NGs was investigated in vivo. For radiolabeling of the NGs, maleimide-1,4,7,10-tetraazacyclododecane-1,4,7,10-tetraacetic acid (maleimide-DOTA) was covalently attached to the pre-polymer prior to NG synthesis (Figure S10B). We have

previously shown that the covalent attachment of DOTA for radiolabeling does not affect the original NG characteristics.[1b] The NGs were then radiolabeled with 120 MBq ^{68}Ga (half-life=68 minutes). Concentration-dependent NG radiolabeling with $\geq 95\%$ yield was achieved with a NG concentration of 0.2 mg (Figure S10 and S11A). Before injecting in vivo, we assessed the NGs stability in the presence of serum and PBS. Our results do not indicate loss of radiolabeling yield for 120 min, demonstrating the stability of our NG (Figure S11B).

Under isoflurane anesthesia, the lateral tail vein of 9 nude mice was injected with 120 μL of NaCl containing 10 ± 3 MBq of different radiolabeled NGs ($n=3$). The PET/CT was acquired 1 h (Figure 8A) and 4 h (Figure 8B) after the injection, which showed higher activity in the blood, demonstrating a longer circulation time in mice injected with soft NGs (Figure 8D). At the end of the second PET/CT scan, the animals were finalized, and the organs were harvested to determine radioactivity using a gamma counter. From the biodistribution profile, represented as the percentage of injected dose per grams of tissue (% ID/g), we observed that the soft reducible NG circulates longer in the blood as compared to hard reducible NG and demonstrates lower liver and spleen uptake comparatively (Figure 8C).
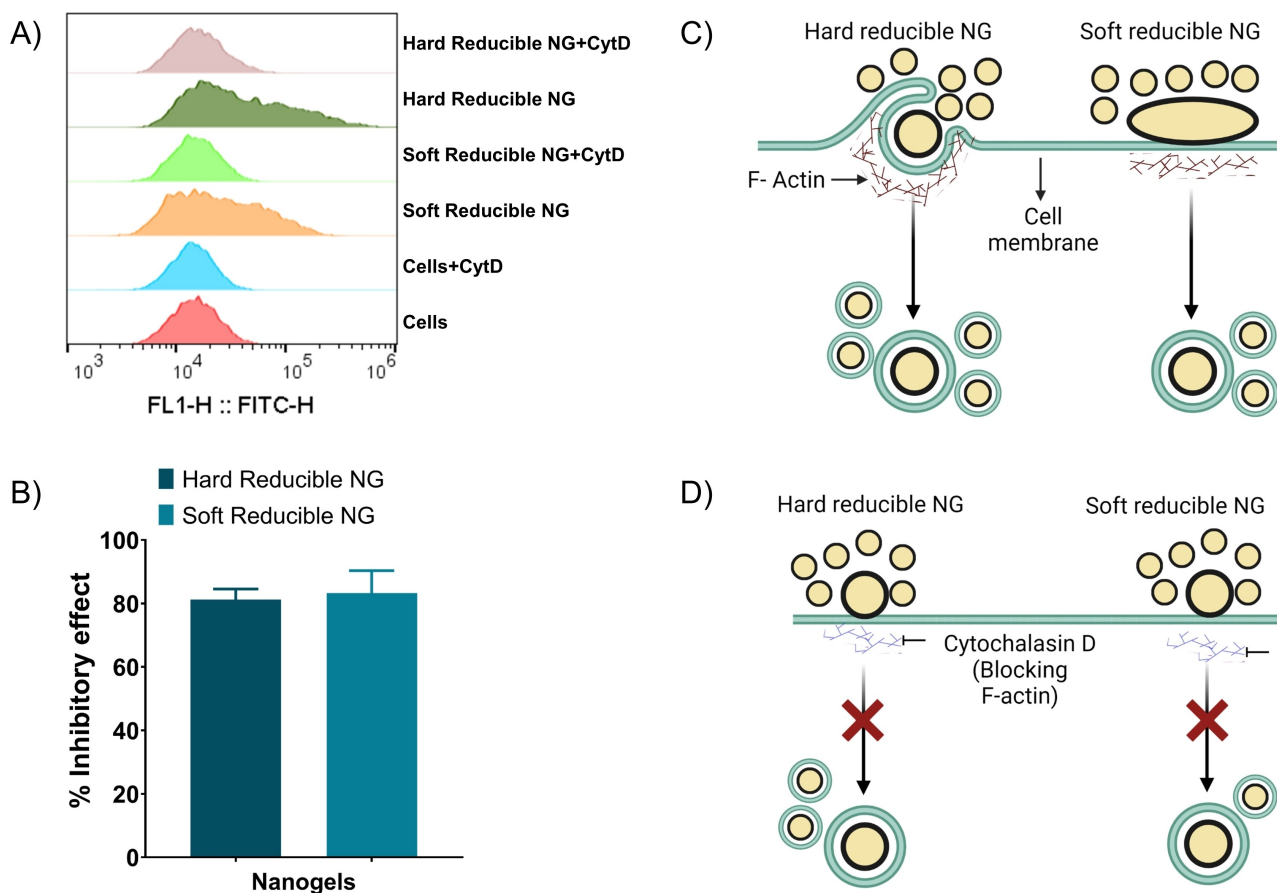
Figure 6. Mechanism of nanogel uptake by stimulated THP-1 cells. A) Flow cytometry histogram of different elastic NGs treated with or without CytD. B) Percentage of NGs cell uptake inhibited upon treating with CytD. C), D) Schematic representing the effect of actin filaments on different elastic NG uptake. C) The presence of actin filaments beneath the cell membrane adds a certain force to the membrane, which deforms the softer NGs, thereby reducing uptake. D) Blocking the actin polymerization by treating the cells with cytochalasin D slows down and reduces the kinetics of cell uptake of the NGs.

The higher activity in the bladder indicates these NG are cleared from the body renally. Moreover, the average activity obtained for the liver (Figure S12), kidneys, and bladder show time-dependent decrease in radioactivity, indicating that the NGs are not retained in these organs, but cleared over time (Figure 8E, F).

This difference in the blood circulation time could be associated with the lower phagocytotic ability of the soft NGs as well as its ability to squeeze through the splenic pores owing to its deformable nature.[4] Due to this difference in the biodistribution between hard and soft NGs, we further analyzed the soft reducible NGs via SDS-PAGE/ phosphor imager analysis, which revealed the presence of an intact NG band in the range of 150–250 kDa after being passed through a membrane with a molecular weight cut-off of 50 kDa (Figure S13A). This validates the ability of the soft NGs to pass through membranes $5\times$ lower than their molecular weight. Furthermore, the molecular weight of the glomerular filtration in the kidney ranges between 30–50 kDa, and it can be hypothesized that the soft NGs can squeeze through the glomerular filtration without being trapped, causing unwanted toxicity.[29] Hendrickson et al., also showed that under pressure differential relevant to

renal filtration, the microgels could pass through pores $10\times$ smaller than their size and remain intact.[30] We speculate that due to the NG deformable characteristics, they can squeeze through the fenestrated capillaries of the kidney and clear via urine, which is further confirmed by PET, showing a decrease in kidney activity over time. In addition, the urine of the mouse (at the time of finalization) from hard and soft reducible NG was analyzed using SDS-PAGE and phosphor imager, which further confirms the clearance of degraded NGs via urine (Figure S13B). This in turn shows that, indeed using degradable NGs, we can achieve faster clearance of the radiolabeled NGs, which will help to decrease the nephrotoxicity associated with PRRT. Here, we have to keep in mind that, although one NG is termed "hard," it is still considered soft compared to conventional nanocarriers studied in drug delivery. Furthermore, no difference in the biodistribution profile between soft reducible and soft non-reducible NG was observed, further confirming the role of NG elasticity in regulating biological processes.
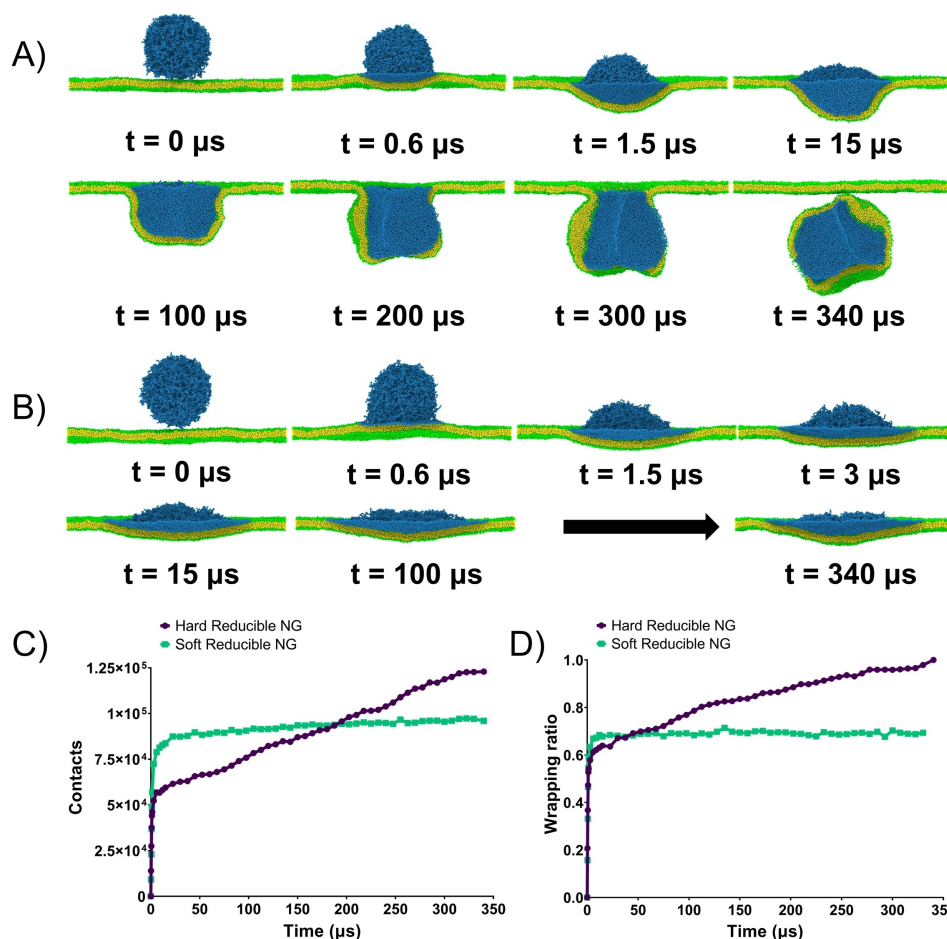
Figure 7. A), B) Simulation snapshots of single hard (A) and soft (B) nanogels at lipid membranes at different simulation times (water molecules are not shown); C), D) number of contacts between NG segments and lipid heads (C) and wrapping ratio (the ratio of NG-membrane contact area to the total area of the NG) as D) functions of simulation time.

Conclusion

We systematically compared the effect of NG elasticity on biodistribution and cellular uptake. The elasticity of NGs was tuned by varying the number of functional groups, while still being able to maintain a similar polymer volume fraction of 44 wt % and a radiolabeling efficiency of $\geq 95\%$. In addition, to eliminate the redox sensitivity of the disulfide NG in a reducing environment, soft non-reducible NG was developed and the NGs with different elasticities were investigated in vitro, in vivo and via computer simulations. This study demonstrated that the biodistribution of the NGs is highly influenced by small changes in the NG elasticity. The longer circulation time of the NG could be due to its lower uptake by the liver/spleen, as demonstrated also in vitro with immune cells. The renal clearance of these NGs highlights the importance of using radiolabeled NGs to decrease nephrotoxicity associated with PRRT. Additionally, via computer simulations we further show that softer the nanogels, the longer is the uptake time. Furthermore, no difference in cell uptake and biodistribution was observed between soft reducible NG and soft non-reducible NG, strengthening the importance NG elasticity plays on drug

delivery processes. In a follow-up study, these nanogels will be radiolabeled with Lutetium-177 to target the somatostatin receptor 2 (SStR2) expressed in neuroendocrine tumors and will be further investigated for nephrotoxicity. In conclusion, for drug delivery, it is vital to design nanocarriers that are minimally phagocytosed to improve overall biodistribution. We emphasize that particles with same size but difference in rigidity have significant difference in cellular uptake. However, we still believe that to have better insight into how elasticity of the NG affects the blood residence time, NGs with smaller steps in modulus should be tested. Another important physiochemical characteristics of nanoparticles is protein opsonisation at the nano-biointerface which plays an important role in blood residence time of the particles. In the case of soft, fussy, hydrophilic NGs, protein opsonins at the interface are considered to be unstable,[31] but we are just beginning to understand these effects. Future studies should be directed towards investigating combination of different physiochemical properties on particle biodistribution. Depending on the target organ an optimum balance among nanocarrier surface chemistry, size, shape, modulus and its effect on circulation time, needs to be reached to improve the outcome of drug delivery.
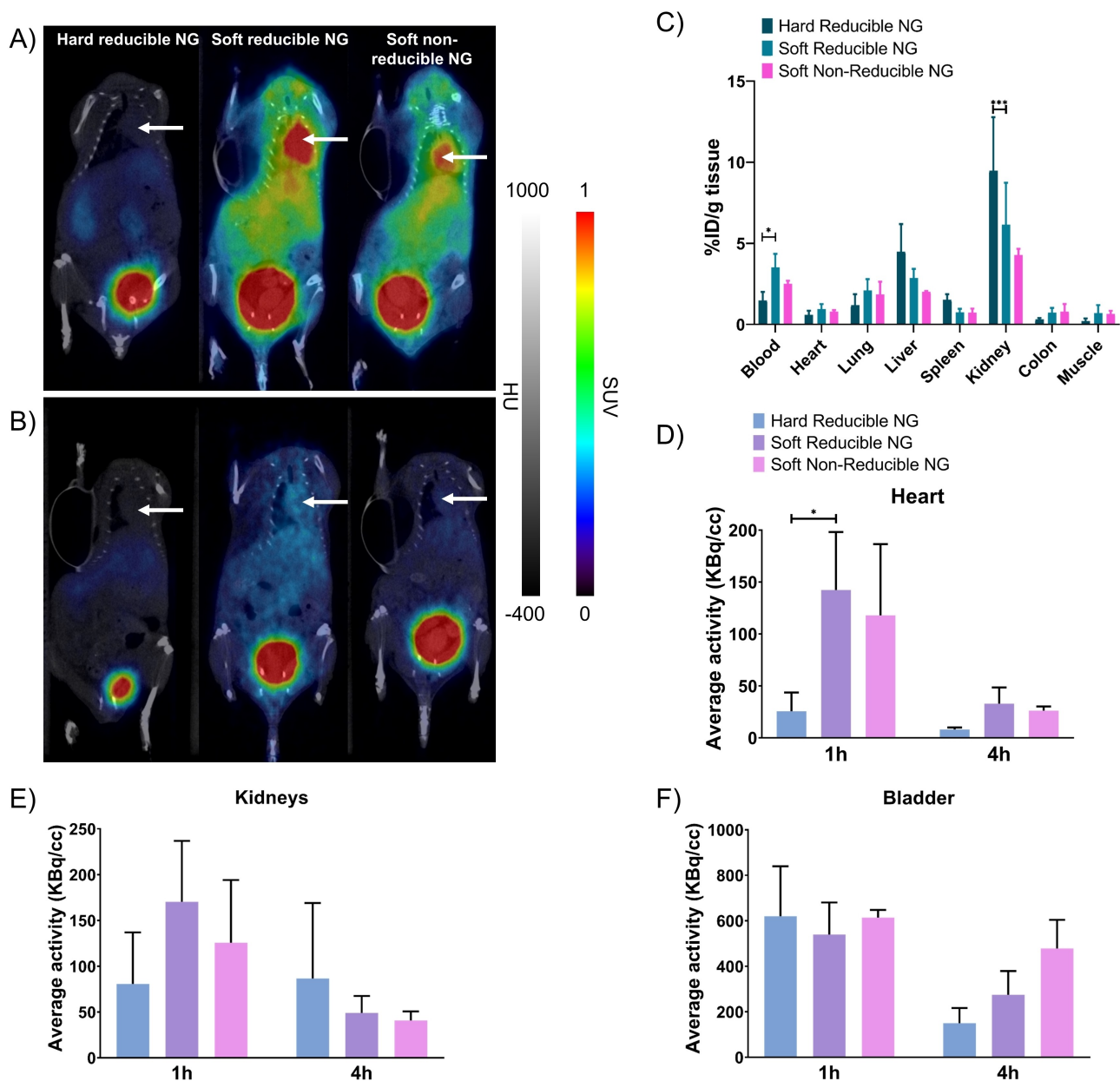
Figure 8. In vivo profiles of different radiolabeled nanogels. A) PET/CT images of radiolabeled NGs injected in vivo at 1 h and B) 4 h post injection (p.i.) showing an increased circulation of soft nanogels. SUV: Standardised uptake value, HU: Hounsfield units. Arrows in white indicate the heart. C) Gamma counter analysis after the last PET/CT of the harvested organs represented as % ID/g tissue. D), E), and F) Average activity (KBq/cc) of the heart, kidneys, and bladder, respectively, was obtained by drawing regions of interest (ROIs) on the whole body images. Values are mean ± SD ($n = 3$). * ($p < 0.05$), *** ($p < 0.001$) as determined by ANOVA.

Conflict of Interest

The authors declare no conflict of interest.

Data Availability Statement

The data that support the findings of this study are available in the Supporting Information of this article.

[1] a) A. Polyak, T. L. Ross, *Curr. Med. Chem.* **2018**, *25*, 4328–4353; b) S. Singh, B. Bingöl, A. Morgenroth, F. M. Mottaghy, M. Möller, J. Schmaljohann, *Macromol. Rapid Commun.* **2013**, *34*, 562–567; c) N. Drude, S. Singh, O. H. Winz, M. Möller, F. M. Mottaghy, A. Morgenroth, *Biomacromolecules* **2017**, *18*, 2489–2498.

[2] a) H. S. Choi, W. Liu, P. Misra, E. Tanaka, J. P. Zimmer, B. I. Ipe, M. G. Bawendi, J. V. Frangioni, *Nat. Biotechnol.* **2007**, *25*, 1165–1170; b) R. K. Jain, *Annu. Rev. Biomed. Eng.* **1999**, *1*, 241–263; c) C. He, Y. Hu, L. Yin, C. Tang, C. Yin, *Biomaterials* **2010**, *31*, 3657–3666; d) K. Xiao, Y. Li, J. Luo, J. S. Lee, W. Xiao, A. M. Gonik, R. G. Agarwal, K. S. Lam, *Biomaterials* **2011**, *32*, 3435–3446; e) M. Danaei, M. Dehghankhold, S. Ataei, F. Hasanzadeh Davarani, R. Javanmard, A. Dokhani, S. Khorasani, M. Mozafari, *Pharmaceutica* **2018**, *10*, 57; f) Y. Geng, P. Dalhaimer, S. Cai, R. Tsai, M. Tewari, T. Minko, D. E. Discher, *Nat. Nanotechnol.* **2007**, *2*, 249–255; g) P. Kolhar, A. C. Anselmo, V. Gupta, K. Pant, B. Prabhakarpandian, E. Ruoslahti, S. Mitragotri, *Proc. Natl. Acad. Sci. USA* **2013**, *110*, 10753–10758; h) S. E. Gratton, P. A. Ropp, P. D. Pohlhaus, J. C. Luft, V. J. Madden, M. E. Napier, J. M. DeSimone, *Proc. Natl. Acad. Sci. USA* **2008**, *105*, 11613–11618; i) X. Huang, L. Li, T. Liu, N. Hao, H. Liu, D. Chen, F. Tang, *ACS Nano* **2011**, *5*, 5390–5399; j) F. Alexis, E. Pridgen, L. K. Molnar, O. C. Farokhzad, *Mol. Pharm.* **2008**, *5*, 505–515; k) J. P. M. Almeida, A. L. Chen, A. Foster, R. Drezek, *Nanomedicine* **2011**, *6*, 815–835.

[3] a) Y. X. Huang, Z. J. Wu, J. Mehrishi, B. T. Huang, X. Y. Chen, X. J. Zheng, W. J. Liu, M. Luo, *J. Cell. Mol. Med.* **2011**, *15*, 2634–2642; b) F. C. Mokken, M. Kedaria, C. P. Henny, M. Hardeman, A. Gelb, *Ann. Hematol.* **1992**, *64*, 113–122.

[4] L. Zhang, Z. Cao, Y. Li, J.-R. Ella-Menye, T. Bai, S. Jiang, *ACS Nano* **2012**, *6*, 6681–6686.

[5] C. Huang, P. J. Butler, S. Tong, H. S. Muddana, G. Bao, S. Zhang, *Nano Lett.* **2013**, *13*, 1611–1615.

[6] a) X. Banquy, F. Suarez, A. Argaw, J.-M. Rabanel, P. Grutter, J.-F. Bouchard, P. Hildgen, S. Giasson, *Soft Matter* **2009**, *5*, 3984–3991; b) A. C. Anselmo, M. Zhang, S. Kumar, D. R. Vogus, S. Menegatti, M. E. Helgeson, S. Mitragotri, *ACS Nano* **2015**, *9*, 3169–3177.

[7] J. Key, A. L. Palange, F. Gentile, S. Aryal, C. Stigliano, D. Di Mascolo, E. De Rosa, M. Cho, Y. Lee, J. Singh, *ACS Nano* **2015**, *9*, 11628–11641.

[8] P. Guo, D. Liu, K. Subramanyam, B. Wang, J. Yang, J. Huang, D. T. Auguste, M. A. Moses, *Nat. Commun.* **2018**, *9*, 130.

[9] a) B. Eshaghi, N. Alsharif, X. An, H. Akiyama, K. A. Brown, S. Gummuluru, B. M. Reinhard, *Adv. Sci.* **2020**, *7*, 2000649; b) A. Garapaty, J. A. Champion, *Bioeng. Transl. Med.* **2017**, *2*, 92–101.

[10] a) X. Wang, L. Li, F. Song, *Crystals* **2021**, *11*, 728; b) Y. Hui, D. Wibowo, Y. Liu, R. Ran, H.-F. Wang, A. Seth, A. P. Middelberg, C.-X. Zhao, *ACS Nano* **2018**, *12*, 2846–2857.

[11] P. Sabourian, G. Yazdani, S. S. Ashraf, M. Frounchi, S. Mashayekhan, S. Kiani, A. Kakkar, *Int. J. Mol. Sci.* **2020**, *21*, 8019.

[12] S. Singh, I. Zilkowski, A. Ewald, T. Maurell-Lopez, K. Albrecht, M. Moller, J. Groll, *Macromol. Biosci.* **2013**, *13*, 470–482.

[13] N. G. Sosale, T. Rouhiparkouhi, A. M. Bradshaw, R. Dimova, R. Lipowsky, D. E. Discher, *Blood* **2015**, *125*, 542–552.

[14] A. C. Anselmo, S. Mitragotri, *Adv. Drug Delivery Rev.* **2017**, *108*, 51–67.

[15] J. Groll, S. Singh, K. Albrecht, M. Moeller, *J. Polym. Sci. Part A* **2009**, *47*, 5543–5549.

[16] X. Huang, D. P. Cavalcante, H. E. Townley, *J. Nanopart. Res.* **2020**, *22*, 1–13.

[17] M. Daigneault, J. A. Preston, H. M. Marriott, M. K. Whyte, D. H. Dockrell, *PLoS One* **2010**, *5*, e8668.

[18] Y. Hui, X. Yi, F. Hou, D. Wibowo, F. Zhang, D. Zhao, H. Gao, C.-X. Zhao, *ACS Nano* **2019**, *13*, 7410–7424.

[19] C. Contini, M. Schneemilch, S. Gaisford, N. Quirke, *J. Exp. Nanosci.* **2018**, *13*, 62–81.

[20] a) M. J. Footer, J. W. Kerssemakers, J. A. Theriot, M. Dogterom, *Proc. Natl. Acad. Sci. USA* **2007**, *104*, 2181–2186; b) T. Yue, X. Zhang, F. Huang, *Soft Matter* **2014**, *10*, 2024–2034.

[21] a) S. R. Heidemann, S. Kaech, R. E. Buxbaum, A. Matus, *J. Cell Biol.* **1999**, *145*, 109–122; b) G. T. Charras, C.-K. Hu, M. Coughlin, T. J. Mitchison, *J. Cell Biol.* **2006**, *175*, 477–490; c) R. Simson, E. Wallraff, J. Faix, J. Niewöhner, G. Gerisch, E. Sackmann, *Biophys. J.* **1998**, *74*, 514–522.

[22] a) X. Yi, X. Shi, H. Gao, *Phys. Rev. Lett.* **2011**, *107*, 098101; b) X. Yi, H. Gao, *Soft Matter* **2015**, *11*, 1107–1115.

[23] J. Sun, L. Zhang, J. Wang, Q. Feng, D. Liu, Q. Yin, D. Xu, Y. Wei, B. Ding, X. Shi, X. Jiang, *Adv. Mater.* **2015**, *27*, 1402–1407.

[24] J. A. Champion, S. Mitragotri, *Proc. Natl. Acad. Sci. USA* **2006**, *103*, 4930–4934.

[25] X. Song, J. Ma, T. Long, X. Xu, S. Zhao, H. Liu, *ACS Appl. Mater. Interfaces* **2021**, *13*, 123–134.

[26] Z. Shen, H. Ye, X. Yi, Y. Li, *ACS Nano* **2019**, *13*, 215–228.

[27] F. Camerin, M. A. N. Fernández-Rodríguez, L. Rovigatti, M.-N. Antonopoulou, N. Gnan, A. Ninarello, L. Isa, E. Zaccarelli, *ACS Nano* **2019**, *13*, 4548–4559.

[28] L. Hoppe Alvarez, S. Eisold, R. A. Gumerov, M. Strauch, A. A. Rudov, P. Lenssen, D. Merhof, I. I. Potemkin, U. Simon, D. Wöll, *Nano Lett.* **2019**, *19*, 8862–8867.

[29] A. Ruggiero, C. H. Villa, E. Bander, D. A. Rey, M. Bergkvist, C. A. Batt, K. Manova-Todorova, W. M. Deen, D. A. Scheinberg, M. R. McDevitt, *Proc. Natl. Acad. Sci. USA* **2010**, *107*, 12369–12374.

[30] a) T. J. Merkel, S. W. Jones, K. P. Herlihy, F. R. Kersey, A. R. Shields, M. Napier, J. C. Luft, H. Wu, W. C. Zamboni, A. Z. Wang, *Proc. Natl. Acad. Sci. USA* **2011**, *108*, 586–591; b) G. R. Hendrickson, L. A. Lyon, *Angew. Chem. Int. Ed.* **2010**, *49*, 2193–2197; *Angew. Chem.* **2010**, *122*, 2239–2243.

[31] S. Abbina, L. E. Takeuchi, P. Anilkumar, K. Yu, J. C. Rogalski, R. A. Shenoi, I. Constantinescu, J. N. Kizhakkedathu, *Nat. Commun.* **2020**, *11*, 1–12.

[32] V. V. Voevodin, A. S. Antonov, D. A. Nikitenko, P. A. Shvets, S. I. Sobolev, I. Y. Sidorov, K. S. Stefanov, V. V. Voevodin, S. A. Zhumatiy, *Supercomput. Front. Innov.* **2019**, *6*, 4–11.